RESEARCH ARTICLE | AUGUST 26 2025

# A phase jump phenomenon within the beat signal for dynamic target measurement in frequency-sweeping interferometry

Wenjun Chen; Xiaoping Li; Zhongwen Deng ; Shuwei Zhang; Haifeng Sun; Lin Li; Hengkang Zhang ; Li Wang; Hai Gong; Herman Koara ; Gleb Vdovin



*Appl. Phys. Lett.* 127, 081103 (2025)
https://doi.org/10.1063/5.0289796

Applied Physics Letters ARTICLE pubs.aip.org/aip/apl

# A phase jump phenomenon within the beat signal for dynamic target measurement in frequency-sweeping interferometry

Cite as: Appl. Phys. Lett. **127**, 081103 (2025); doi: 10.1063/5.0289796
Submitted: 9 July 2025 · Accepted: 5 August 2025 ·
Published Online: 26 August 2025



Wenjun Chen,[1] Xiaoping Li,[1] Zhongwen Deng,[1,a)] Shuwei Zhang,[1] Haifeng Sun,[1] Lin Li,[2] Hengkang Zhang,[2] Li Wang,[2] Hai Gong,[3] Herman Koara,[4] and Gleb Vdovin[5,6]

## AFFILIATIONS

[1]School of Aerospace Science and Technology, Xidian University, Xi'an 710000, China
[2]Space Optoelectronic Measurement and Perception Lab, Beijing Institute of Control Engineering, Beijing 100190, China
[3]Huzhou Research Institute of Zhejiang University, Zhejiang University, Huzhou 313000, China
[4]College of Control Science and Engineering, Zhejiang University, Hangzhou 310000, China
[5]Faculty of Mechanical Engineering, Delft University of Technology, Mekelweg 2, 2628CD Delft, The Netherlands
[6]Flexible Optical BV, Polakweg 10-11, 2288GG Rijswijk, The Netherlands

[a)]**Author to whom correspondence should be addressed:** zwdeng@xidian.edu.cn

## ABSTRACT

Frequency-sweeping interferometry (FSI) is an advanced coherent measurement technique capable of simultaneous high-precision measurement of dynamic target absolute distance and velocity. This study reveals that the dynamic target modulates the beat signal in FSI, causing the phase jump phenomenon in the beat signal and subsequent measurement failures. We theoretically derive and experimentally validate the conditions for phase jumps. Additionally, we propose using time-frequency analysis methods to detect phase jump instants and reconstruct the instantaneous frequency trajectory of the beat signal modulated by phase jumps. Experimental results show that even with phase jumps, we achieved a dynamic velocity measurement of −135.40 mm/s on a 0.5 m baseline, surpassing the theoretical limit of −4.40 mm/s under this baseline, while maintaining effective measurement capability on an extended 10 m baseline. The discovery and resolution of phase jumps are expected to overcome velocity limitation in FSI, significantly expanding its velocity measurement range.





Frequency-sweeping interferometry (FSI) enables the precise measurement of absolute distance and velocity for dynamic targets by analyzing the time–frequency (T–F) characteristics of the beat signal, which has been proposed for application in high-precision inter-satellite ranging within distributed satellite formations for the "MEAYIN" and "Darwin" space observation projects.[1,2] Additionally, it has found widespread applications in large-scale equipment manufacturing,[3–5] biomedical imaging,[6,7] and autonomous driving,[8–10] with particularly notable applications in dynamic target detection.[4,5,11–15] However, we discovered that dynamic targets can modulate the phase of the beat signal, causing phase jumps in the beat signal. Consequently, the T–F information derived from the beat signal may not accurately represent the true motion state of the target, thereby affecting the ability of FSI to measure dynamic targets. This study presents comprehensive theoretical derivations and experimental validations of this phenomenon, along with proposing T–F analysis methods to identify phase jump instants and recover the instantaneous frequency (IF) trajectory of beat signal influenced by phase jumps. The discovery and resolution of phase jump phenomena effectively extends the velocity measurement range of FSI systems.

The schematic of FSI is illustrated in Fig. 1(a). The beat signal [as shown in Fig. 1(b)] sampled by the analog-to-digital converter is expressed as[2,14,15]

$$I(t) = \cos\left[\frac{4\pi n}{c}(\upsilon_0 + \beta(t)t) \cdot L(t)\right], \tag{1}$$

where $\upsilon_0$ represents the initial laser frequency, $\beta(t)$ denotes the frequency-sweeping rate, $n$ is the refractive index of air, $c$ is the speed of light, and $L(t)$ is the absolute distance. When the target is stationary, $L(t)$ remains constant, the instantaneous frequency (IF) of the beat signal can be expressed as

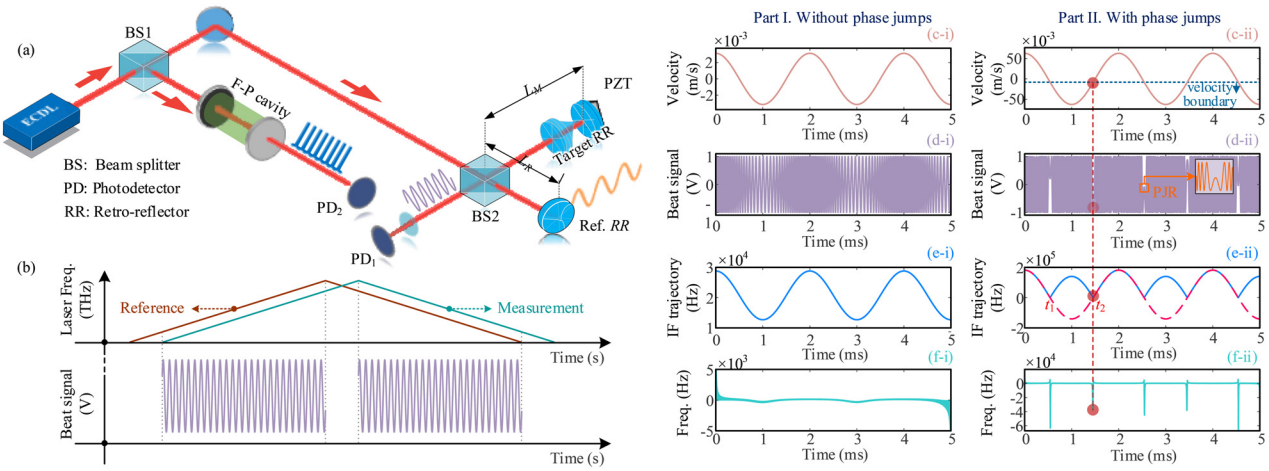


**FIG. 1.** (a) The schematic of the FSI system. (b) Principle of beat signal formation. (c) The movement pattern and velocity of the target. (d) Beat signal. (e) IF trajectory of beat signal. (f) T–F distribution of IF trajectory. (i) Without phase jumps and (ii) with phase jumps. PJR: phase jump region.

$$f_b(t) = \frac{2n\beta(t)}{c} \cdot L(t). \tag{2}$$

However, in dynamic target measurements, $L(t)$ is no longer fixed. When a target moves along the measurement optical axis, the IF of the beat signal [as shown in Fig. 1(d)] is expressed as

$$f_b(t) = \frac{2n}{c}\left[\beta(t)L(t)+\upsilon(t)L'(t)\right], \tag{3}$$

where $\upsilon(t) = \upsilon_0 + \beta(t)t$ is the instantaneous laser frequency, and $L'(t)$ is the instantaneous velocity of the target along the measurement optical axis.

It is important to note that the sign of $L'(t)$ is related to the moving direction of the target. When the target moves away from the BS2, $L'(t) > 0$; conversely, $L'(t) < 0$ when it moves toward the BS2. This implies two possible scenarios for $f_b(t)$:

(1) When the target is moving at a low velocity [see Figs. 1(c)–1(i)], no matter how it moves along the measurement optical axis, the value of $|\upsilon(t)L'(t)|$ remains less than $|\beta(t)L(t)|$, ensuring that $\beta(t)L(t)+\upsilon(t)L'(t) > 0$ always holds. In this case, the beat signal and its IF trajectory are shown in Figs. 1(d)–1(i) and 1(e)–1(i), respectively.
(2) As $|L'(t)|$ increases [see Fig. 1(c-ii)], $|\beta(t)L(t)|$ may become less than $|\upsilon(t)L'(t)|$. When the target moves toward the BS2 ($L'(t) < 0$) and $L'(t)$ exceeds the velocity boundary, resulting in $\beta(t)L(t)+\upsilon(t)L'(t) < 0$. As illustrated in Fig. 1(e-ii), the velocity of target modulates the IF trajectory of beat signal, causing $f_b(t)$ to transition between positive and negative values at times $t_1$ and $t_2$. As depicted in Fig. 1(d-ii), the abrupt transition in $f_b(t)$ leads to phase jumps in the beat signal.

It is noteworthy that the sign of the $\beta(t)$ is related to the frequency sweep direction of the laser. Based on the above-mentioned analysis, the velocity boundary for the phase jumps is defined as

$$\begin{cases} L'(t) < -\beta(t)L(t)/\upsilon(t), & (\beta(t) > 0), \\ L'(t) > -\beta(t)L(t)/\upsilon(t), & (\beta(t) < 0). \end{cases} \tag{4}$$

Equation (4) indicates that phase jumps will occur in the beat signal when the target velocity along the measurement optical axis exceeds the velocity boundary, regardless of the frequency sweep direction. The beat signal (with phase jumps) and phase jump region are shown in Fig. 1(d-ii). The phase jumps introduce uncertainty in the phase of the beat signal,[16] affecting the accuracy and reliability of the FSI system. This phenomenon poses a technical challenge to FSI dynamic measurement.

The velocity thresholds causing phase jumps during both upward and downward laser frequency sweeps are presented in Figs. 2(a) and 2(b), respectively. The colored areas represent the regions without phase jumps. When the target vibration velocity exceeds the colored region, i.e., satisfies the condition in Eq. (4), the phase jumps will occur in the beat signal. As illustrated in Fig. 2(c), phase jumps significantly broaden the spectrum peak of the beat signal, making it impossible to directly extract the distance and velocity of the target from the beat signal. Although increasing the laser center wavelength $\lambda$ or measurement baseline $L$ can delay this phenomenon, it cannot be completely prevented.

To suppress the impact of phase jumps on dynamic measurements, we further analyze its mechanism on the beat signal. Theoretically, the IF trajectory should follow the dashed line shown in Fig. 3(b). However, due to phase jumps, the IF trajectory originally on the negative half-axis folds onto the positive half-axis,[17] as depicted by the solid line in Fig. 3(b). Based on this analysis, accurately reconstructing the IF trajectory is crucial for suppressing the impact of phase jumps. The key to this reconstruction is precisely identifying the phase jump instants, which can be determined by analyzing the IF trajectory, as its characteristics are dictated by the phase structure of the beat signal.[18]

Notably, the T–F analysis results of the IF trajectory reveal a significant abrupt change at the phase jump instants, as shown in Fig. 1(f-ii). This property enables the possibility for determining the phase jump instants and recovering the IF trajectory. To verify this specific T–F characteristic, a T–F analysis model was constructed.[19–21] The IF trajectory of beat signal is expressed as

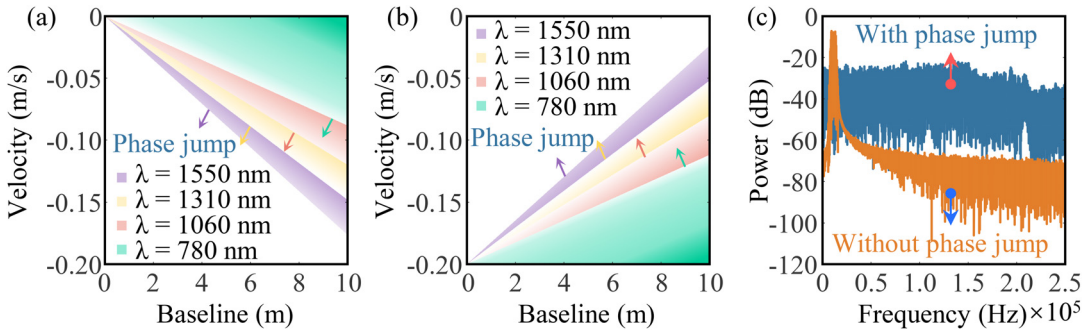


**FIG. 2.** Velocity threshold distribution for phase jumps in FSI: (a) up-sweep ($\beta(t) > 0$) and (b) down-sweep ($\beta(t) < 0$). Colored regions: without phase jumps regions. (c) Spectrum of the beat signal.

$$a(t) = \begin{cases} Ae^{j\omega_1 t+\phi_0}, & t < t_0 \\ Ae^{j\omega_1 t+(\phi_0+\phi)}, & t \geq t_0 \end{cases}, \tag{5}$$

where $t_0$ is the instant of phase jump, $A$ is the amplitude, $\Delta\phi$ is the magnitude of the phase change, and $\omega_1$ is the instantaneous frequency of $a(t)$, which is sampled by a rectangular window. As the window slides, three possible results arise for the T–F analysis:

(1) When the rectangular window does not cover a phase jump instant, the result for $a(t)$ is

$$\begin{aligned} G(t,\omega) &= \int_{-T/2}^{T/2} a\left(t+\frac{\eta}{2}\right)s^*\left(t-\frac{\eta}{2}\right)\cdot e^{-j\omega\eta}d\eta \\ &= A^2\cdot\frac{2\cdot\left(\sin(\omega-\omega_1)\frac{T}{2}\right)}{\omega-\omega_1}, \end{aligned} \tag{6}$$

where $s(\cdot)$ represents the time-frequency window function and $T$ is the width of the rectangular window. When $\omega \to \omega_1$, $G(t,\omega)$ is expressed as

$$\lim_{\omega\to\omega_1} G(t,\omega) = A^2\cdot T, \tag{7}$$

in this case, $G(t,\omega)$ remains constant, as shown in Fig. 3(c).

(2) When the phase jump instant occurs within the rectangular window and coincides with its center, the $G(t,\omega)$ is expressed as

$$G(t,\omega) = \frac{A^2\left[\sin\left((\omega-\omega_1)\frac{T}{2}+\phi\right)-\sin\phi\right]}{\omega-\omega_1}, \tag{8}$$

when $\omega \to \omega_1$, Eq. (8) is expressed as

$$\lim_{\omega\to\omega_1} G(t,\omega) = A^2T\cos(\Delta\phi), \tag{9}$$

which indicates that, at the phase jump instant, the value of $G(t,\omega)$ undergoes a significant change, as illustrated in Fig. 3(c).

(3) When the phase jump instant occurs within the rectangular window but is offset from the center by $\varepsilon$, then $G(t,\omega)$ is expressed as

$$G(t,\omega) = \frac{\varepsilon A^2\sin(\omega-\omega_1)}{\omega-\omega_1} + h(\omega), \tag{10}$$

where $h(\omega)$ is expressed as

$$h(\omega) = \int_{-\frac{\varepsilon}{2}}^{\frac{T}{2}} 2A^2\cos[(\omega-\omega_1)\varsigma]d\varsigma, \tag{11}$$

when $\omega \to \omega_1$, Eq. (12) is expressed as

$$\lim_{\omega\to\omega_1} G(t,\omega) = A^2\varepsilon + A^2(T-\varepsilon)\cos(\Delta\phi), \tag{12}$$

which indicates that near the phase jump instant, $G(t,\omega)$ exhibits a broken linear trend with $\varepsilon$, reaching a minimum at the phase jump instant.

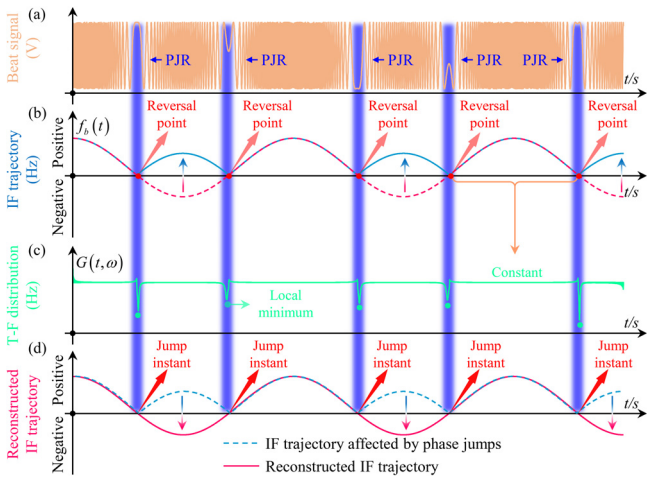


**FIG. 3.** Signal analysis and processing procedure. (a) Beat signal (with phase jumps). (b) IF trajectory of the beat signal. (c) T–F distribution of IF trajectory. (d) Reconstructed IF trajectory.

As we can see in Fig. 1(f-i), if without phase jumps in the beat signal, the T–F distribution of the IF trajectory is a smooth curve (without abrupt changes). In contrast, when phase jumps occur in the beat signal, the T–F distribution exhibits distinct jump values, as illustrated in Fig. 1(f-ii), where the local minimum values precisely match the phase jump instants in the IF trajectory. These results are consistent with the

theoretical derivation of the constructed T–F analysis model. Thus, with the T–F analysis methods, we can identify the phase jump instants $t_1, t_2, \ldots, t_n$, with the process flow illustrated in Fig. 3. The IF trajectory reconstruction function is expressed as

$$\kappa(t) = \begin{cases} -1, & t_i < t < t_{i+1}, \\ 1, & t_{i+1} < t < t_{i+2}. \end{cases} \tag{13}$$

Here, $[t_i, t_{i+1}]$ $(t_1, t_2, \ldots, t_n)$ is the interval in which the IF trajectory flips, and the reconstructed IF trajectory [see in Fig. 3(d)] is expressed as

$$R(t) = a(t) \cdot \kappa(t). \tag{14}$$

The reconstructed IF trajectory will be used to demodulate the absolute distance $L(t)$ and velocity $L'(t)$ of a dynamic target.

To further validate the effectiveness of detecting phase jump instants and recovering IF trajectories affected by phase jumps using T–F analysis, we conducted a proof-of-concept vibration measurement experiment. The experimental system is shown in Fig. 4(a). An external cavity diode laser (ECDL, TLB6712, Newport) with a center wavelength of 780 nm was employed as the laser source. Frequency sweep linearization was performed on the

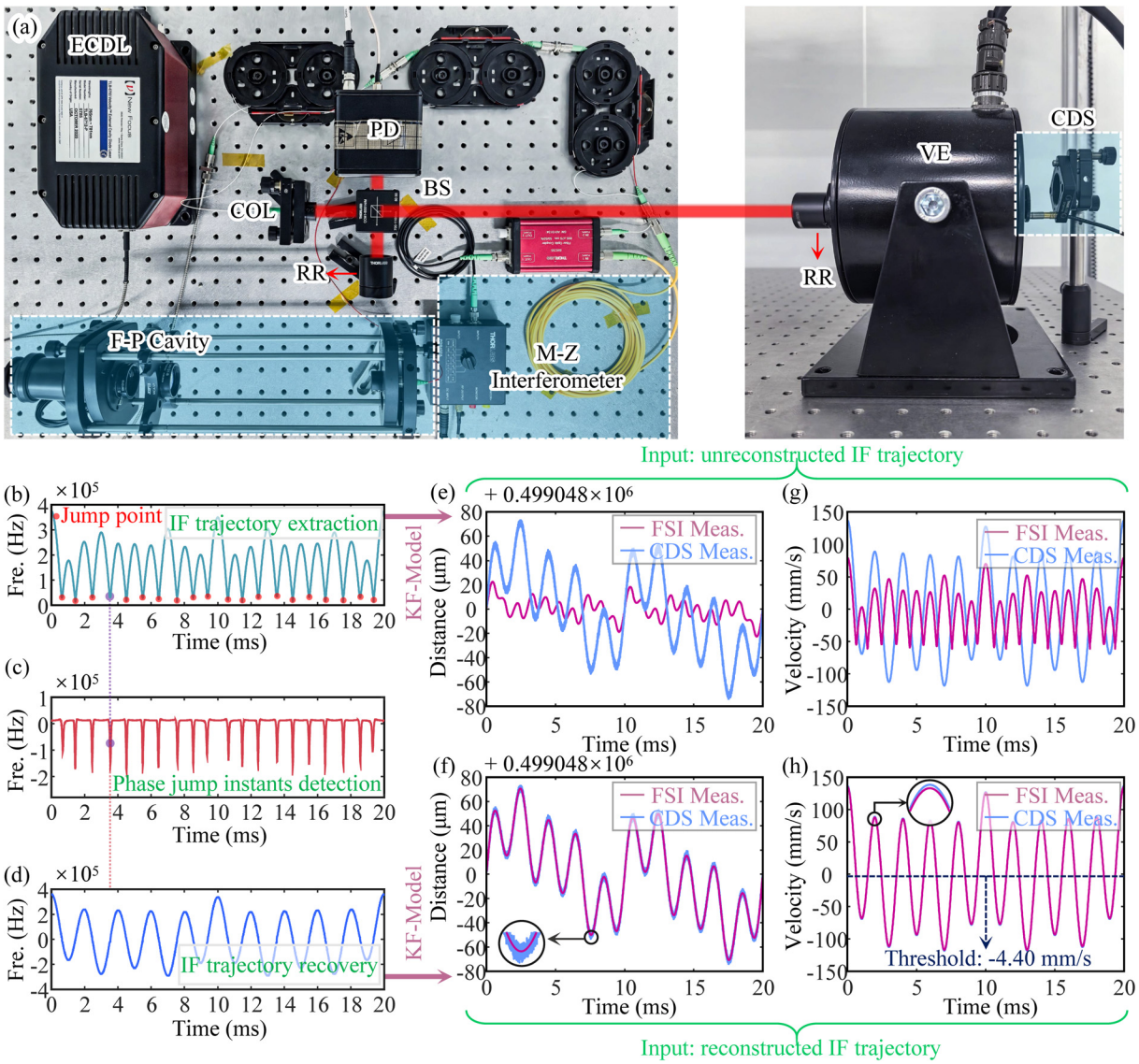


**FIG. 4.** (a) Experimental setup of the measurement system. (b) IF trajectory of the beat signal (with phase jumps). (c) T–F distribution of IF trajectory. (d) Reconstructed IF trajectory. (e) KF model-based FSI vibration measurement results (Input: unreconstructed IF trajectory). (f) KF model-based FSI vibration measurement results (Input: reconstructed IF trajectory). (g) KF model-based FSI velocity measurement results (Input: unreconstructed IF trajectory). (f) KF model-based FSI velocity measurement results (Input: reconstructed IF trajectory).

ECDL prior to the experiment.[2] An F-P Cavity (SA200, Thorlabs) and a Mach–Zehnder (M–Z) interferometer were used to monitor $\upsilon(t)$ and $\beta(t)$. The beat signals were detected by a photodetector (PD, 1801-FS, Newport) and synchronously collected with F-P signals using a data acquisition card (NI-PXle-5105) at 60 MS/s. A vibration exciter (VE) (SA-JZ020, SHIAO; max amplitude: ±10 mm; and frequency range: DC-4 kHz) induces vibrations in the target retro-reflector. To synchronously monitor the vibrations of the target retro-reflector, a capacitive displacement sensor (CDS) (Micro-Epsilon, capaNCDT DL6220-CS02; dynamic resolution: 4 nm) serves as an external reference. The positions of the VE and CDS are shown in Fig. 4(a).

In signal processing, a T–F analysis algorithm based on the multi-synchrosqueezing transform[19] was employed to extract the IF trajectory of the beat signal. The extracted IF trajectory of the beat signal, affected by phase jumps, is shown in Fig. 4(b), where the trajectory that should be in the negative half-axis flips to the positive half-axis. Additionally, the T–F distribution of the IF trajectory, presented in Fig. 4(c), reached local minimum values at the phase jump instants, perfectly aligning with those in the IF trajectory. The experimental results are highly consistent with the theoretical analysis. Finally, the IF trajectory was reconstructed by Eq. (14), with the results displayed in Fig. 4(d). The reconstructed IF trajectory will serve as input for the Kalman filter (KF)-based FSI model to demodulate the target's motion state.[22,23]

The vibration measurement results on the 0.5 m baseline are shown in Figs. 4(e) and 4(f). Directly inputting the IF trajectory with phase jumps into the KF-based FSI system leads to significant measurement deviations [Fig. 4(e)], indicating that phase jumps degrade the accurate measurement of target motion state. Comparatively, after reconstructing the IF trajectory, the FSI system measurement results were closely aligned with the CDS measurement results [Fig. 4(f)], with a maximum error of less than 4.5 $\mu m$. The reconstruction of the IF trajectory enables accurate measurement of the dynamic target with a maximum amplitude of 70.74 $\mu m$. Additionally, the velocity measurements before and after IF trajectory reconstruction are shown in Figs. 4(g) and 4(h). After reconstructing the IF trajectory, FSI accurately measured the velocity of the dynamic target, achieving a maximum velocity of −135.40 mm/s, which significantly surpasses the theoretical velocity limit of −4.40 mm/s for the FSI system under current experimental conditions.

To further demonstrate the nonrandomness of the phase jumps phenomenon in FSI, we extended the measurement baseline and adjusted the VE output amplitude. The beat signal and the reconstructed IF trajectory are shown in Fig. 5(a), where phase jumps still exist in the beat signal. We estimated the motion state of the retro-reflector (RR) as shown in Fig. 5(b), with vibration amplitude and frequency values of 289.376 $\mu m$ and 96.484 Hz, respectively. When compared to the reference values in Fig. 5(c), the relative errors in amplitude and frequency are 6.96% and 0.303%, respectively. Furthermore, as shown in Fig. 5(b), on the 9.752959 m baseline, the velocity threshold that induces phase jumps increased to −86.00 mm/s. However, after reconstructing the IF trajectory, the maximum measured velocity reached −179.61 mm/s. The experimental results further demonstrate the existence of phase jumps and the effectiveness of the T–F analysis method in FSI dynamic target measurement.

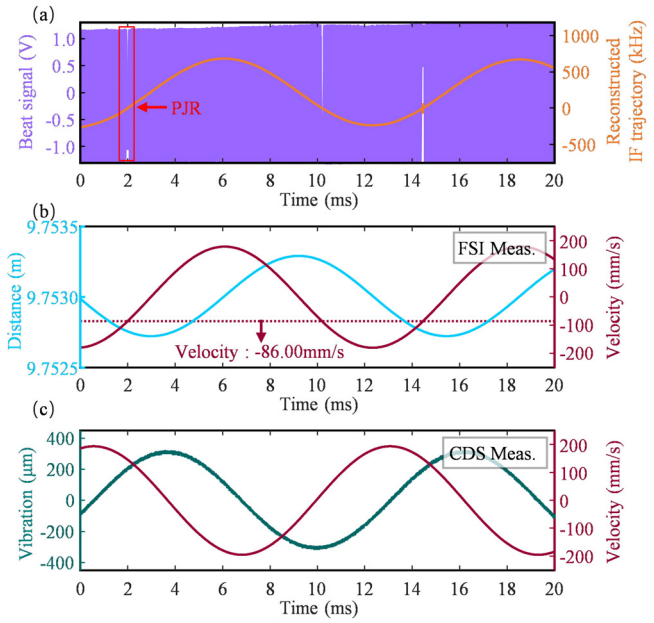


**FIG. 5.** (a) Beat signal (with phase jumps). (b) The measurement results from FSI system. (c) The measurement results of vibration from CDS.

In summary, this study theoretically derives and experimentally verifies the phase jumps phenomenon in beat signal during FSI measurements of dynamic targets, establishing the quantitative condition [Eq. (4)]. To address this issue, we propose using T–F analysis methods to detect phase jump instants and reconstruct the IF trajectory (with phase jumps). The validity of employing such methods is also demonstrated. Experimental results demonstrate that a dynamic velocity measurement of −135.40 mm/s was achieved on a 0.5 m baseline, surpassing the theoretical limit of −4.40 mm/s by nearly 30 times, while maintaining effective measurement capability on an extended 10 m baseline. This study holds promise for overcoming velocity limitations in FSI measurements and significantly expanding the dynamic measurement range of FSI. However, the main limitation of the current method is that the accuracy in detecting phase jump instants and reconstructing IF trajectory is influenced by the signal-to-noise ratio. Future research could focus on using more advanced signal processing techniques or developing sophisticated experimental systems to mitigate the effect of phase jumps on FSI dynamic measurements. This research is anticipated to substantially enhance the dynamic measurement capabilities of FSI, with promising practical application in the "MEAYIN" space project.

This study was supported by the National Natural Science Foundation of China (NSFC) (52205576), the Optoelectronic Measurement and Intelligent Perception Zhongguancun Open Lab (No. LabSOMP-2023-04), the Key Research and Development Program of Shaanxi (Program No. 2025CY-YBXM-121), and the State Key Laboratory for Manufacturing Systems Engineering (Grant No. klms2021005). Hai Gong would like to acknowledge support from the National Natural Science Foundation of China (NSFC) (12204409).

## AUTHOR DECLARATIONS

### Conflict of Interest

The authors have no conflicts to disclose.

### Author Contributions

**Wenjun Chen:** Conceptualization (equal); Data curation (equal); Formal analysis (equal); Methodology (equal); Software (equal); Writing – original draft (equal). **Xiaoping Li:** Funding acquisition (equal); Project administration (equal); Supervision (equal). **Zhongwen Deng:** Conceptualization (equal); Supervision (equal); Validation (equal); Writing – review & editing (equal). **Shuwei Zhang:** Data curation (equal); Investigation (equal); Methodology (equal). **Haifeng Sun:** Conceptualization (equal); Data curation (equal); Project administration (equal); Supervision (equal); Writing – original draft (equal). **Lin Li:** Conceptualization (equal); Resources (equal); Supervision (equal). **Hengkang Zhang:** Project administration (equal); Resources (equal); Supervision (equal). **Li Wang:** Project administration (equal); Resources (equal); Supervision (equal). **Hai Gong:** Conceptualization (equal); Funding acquisition (equal); Project administration (equal). **Herman Koara:** Conceptualization (equal); Data curation (equal); Software (equal); Supervision (equal). **Gleb Vdovin:** Conceptualization (equal); Supervision (equal); Validation (equal).

## DATA AVAILABILITY

The data that support the findings of this study are available from the corresponding author upon reasonable request.

## REFERENCES


[1]A. Cabral, M. Abreu, and J. M. Rebordão, "Dual-frequency sweeping interferometry for absolute metrology of long distances," Opt. Eng. **49**, 085601 (2010).

[2]W. Chen, X. Li, Z. Deng, H. Sun, S. Zhang, Y. Liu, and H. Gong, "Data-driven model based self-adaptive frequency-sweeping linearization in frequency-sweeping interferometry for absolute distance measurement," Measurement **253**, 117742 (2025).

[3]J. Dale, B. Hughes, A. J. Lancaster, A. J. Lewis, A. J. H. Reichold, and M. S. Warden, "Multi-channel absolute distance measurement system with sub ppm-accuracy and 20 m range using frequency scanning interferometry and gas absorption cells," Opt. Express **22**, 24869–24893 (2014).

[4]R. Bao, F. Duan, X. Fu, Z. Yu, W. Liu, and G. Guo, "Frequency-scanning interferometry for axial clearance of rotating machinery based on speed synchronization and extended Kalman filter," Opt. Lasers Eng. **164**, 107515 (2023).

[5]X. Cheng, J. Liu, Y. Zhang, F. Zhang, and X. Qu, "Simultaneous measurement of distance and speed via frequency-modulated continuous-wave lidar system based on $H_{13}C_{14}N$ gas cell," Opt. Lasers Eng. **159**, 107193 (2022).

[6]Z. Wang, B. Potsaid, L. Chen, C. Doerr, H.-C. Lee, T. Nielson, V. Jayaraman, A. E. Cable, E. Swanson, and J. G. Fujimoto, "Cubic meter volume optical coherence tomography," Optica **3**, 1496–1503 (2016).

[7]Y. Tang, J. Zhu, L. Zhu, F. Fan, Z. Ma, and F. Zhang, "Blood coagulation monitoring under static and flow conditions with optical coherence tomography autocorrelation analysis," Appl. Phys. Lett. **120**, 163702 (2022).

[8]G. Xu, Y. Wang, S. Xiong, and G. Wu, "Digital-micromirror-device-based surface measurement using heterodyne interferometry with optical frequency comb," Appl. Phys. Lett. **118**, 251104 (2021).

[9]X. Zhang, J. Pouls, and M. C. Wu, "Laser frequency sweep linearization by iterative learning pre-distortion for FMCW lidar," Opt. Express **27**, 9965–9974 (2019).

[10]C. Lin, Y. Wang, Z. Li, and Y. Tan, "All-fiber fast coherent lidar for ranging and velocimetry based on optical comb injection," Appl. Phys. Lett. **125**, 241110 (2024).

[11]K. Kokkonen and M. Kaivola, "Scanning heterodyne laser interferometer for phase-sensitive absolute-amplitude measurements of surface vibrations," Appl. Phys. Lett. **92**, 063502 (2008).

[12]L. Cheng, X. Ziyi, L. Guodong, L. Bingguo, C. Fengdong, G. Yu, and L. Binghui, "Dynamic nonlinearity errors in laser Doppler vibrometer measurements induced by environmental vibration and error correction," Opt. Express **30**, 30705–30717 (2022).

[13]Y. Shang, J. Lin, L. Yang, Y. Liu, T. Wu, Q. Zhou, and J. Zhu, "Precision improvement in frequency scanning interferometry based on suppression of the magnification effect," Opt. Express **28**, 5822–5834 (2020).

[14]H. Liu, W. Zhang, B. Shao, P. Zhang, and W. Chen, "Algorithm of Doppler error suppression in frequency-swept interferometry for the dynamic axial clearance measurement of high-speed rotating machinery," Opt. Express **29**, 42471–42484 (2021).

[15]B. Shao, W. Zhang, P. Zhang, and W. Chen, "Dynamic clearance measurement using fiber-optic frequency-swept and frequency-fixed interferometry," IEEE Photonics Technol. Lett. **32**, 1331–1334 (2020).

[16]Y. Arosa, E. López Lago, and R. de la Fuente, "The phase ambiguity in dispersion measurements by white light spectral interferometry," Opt. Laser Technol. **95**, 23–28 (2017).

[17]L. Stanković, I. Djurović, S. Stanković, M. Simeunović, S. Djukanović, and M. Daković, "Instantaneous frequency in time–frequency analysis: Enhanced concepts and performance of estimation algorithms," Digital Signal Process. **35**, 1–13 (2014).

[18]B. Boashash, "Estimating and interpreting the instantaneous frequency of a signal. I. Fundamentals," Proc. IEEE **80**, 520–538 (1992).

[19]G. Yu, Z. Wang, and P. Zhao, "Multisynchrosqueezing transform," IEEE Trans. Ind. Electron. **66**, 5441–5455 (2019).

[20]M. Kalra, S. Kumar, and B. Das, "Moving ground target detection with seismic signal using smooth pseudo Wigner–Ville distribution," IEEE Trans. Instrum. Meas. **69**, 3896–3906 (2020).

[21]J. Lerga and V. Sucic, "Nonlinear if estimation based on the pseudo WVD adapted using the improved sliding pairwise ICI rule," IEEE Signal Process. Lett. **16**, 953–956 (2009).

[22]Z. Deng, Z. Liu, X. Jia, W. Deng, and X. Zhang, "Dynamic cascade-model-based frequency-scanning interferometry for real-time and rapid absolute optical ranging," Opt. Express **27**, 21929–21945 (2019).

[23]L. Tao, Z. Liu, W. Zhang, and Y. Zhou, "Frequency-scanning interferometry for dynamic absolute distance measurement using Kalman filter," Opt. Lett. **39**, 6997–7000 (2014).